

## Supporting Information

### **A tetrahedron-shaped polyoxoatomotungstate encapsulating a hexanuclear octahedral lanthanide-oxo cluster for an amperometric bromate sensor**

Lan Yu, Jing Ye, Da-Huan Li, Yan-Qiong Sun\*, Xin-Xiong Li and Shou-Tian Zheng\*  
College of Chemistry, Fuzhou University, Fuzhou, Fujian 350108, China.

\*Email: [sunyq@fzu.edu.cn](mailto:sunyq@fzu.edu.cn); [stzheng@fzu.edu.cn](mailto:stzheng@fzu.edu.cn)

#### Contents

1. Materials and Methods
2. Additional Tables
3. Additional Figures

#### **1. Materials and Methods**

##### **Instruments**

Powder X-ray diffraction (PXRD) patterns were measured using a Rigaku DMAX 2500 diffractometer with  $\text{CuK}_\alpha$  radiation ( $\lambda = 1.54056 \text{ \AA}$ ) in the range of  $3\text{--}50^\circ$ .

FT-IR spectra were determined in the range of  $4000\text{--}500 \text{ cm}^{-1}$  on an Opus Vertex 70 FT-IR infrared spectrophotometer.

The UV-vis diffuse reflectance data were obtained with a UV-2600 spectrophotometer (Shimadzu) in the range of  $200\text{--}800 \text{ nm}$  at room temperature.

Thermogravimetric analyses were performed on a Mettler Toledo TGA/SDTA 851<sup>e</sup> analyzer in an  $\text{N}_2$ -flow atmosphere with a heating rate of  $10 \text{ }^\circ\text{C}/\text{min}$  at a temperature of  $30\text{--}1000^\circ\text{C}$ .

Energy dispersive spectrometry (EDS) analyses were carried out on a Hirox SH-4000 M type desktop scanning electron microscope.

Electrochemical experiments were accomplished using a CHI 660 electrochemical workstation equipped with a standard three-electrode system using  $0.1 \text{ mol/L H}_2\text{SO}_4$  as the electrolyte, with Pt wire as the counter electrode, the modified glassy carbon electrode (GCE) as the working electrode, and the Ag/AgCl electrode as the reference electrode.

##### **Preparation for working electrode**

MWCNTs (multi-walled carbon nanotubes) were used as carriers for the preparation of complex-modified electrodes by electrostatic assembly method.  $50 \text{ mg}$  of MWCNTs were weighed and immersed in  $20\% \text{ HNO}_3$  for  $12 \text{ h}$ , then filtered and washed several times with water to pH neutral. The MWCNTs were dried at  $70^\circ\text{C}$  and placed in a clean round-bottomed flask containing

30 mL of concentrated sulfuric acid and 10 mL of concentrated nitric acid, and then refluxed in an oil bath at 80 °C for 2h. Finally, it was filtered and washed with water until the filtrate was neutral, and the resulting MWCNTs were dried under vacuum at 70 °C.

Then 10 mg of the above pretreated MWCNTs were ultrasonically dispersed in 20 mL of a mixed solution containing 0.25% poly-diallyldimethyl ammonium chloride (PDDA) and 0.5 mol/L NaCl and sonicated for 40 min. The dispersion was centrifuged and washed three times, and finally re-dispersed in 5 mL of deionized water to obtain the PDDA-MWCNTs dispersion.

The glassy carbon electrodes (3mm) were ground and allowed to dry naturally. 10 µL of the PDDA-MWCNTs complex was first drop-coated on the electrode surface and left at room temperature for 30 min to prepare GCE.

Then 10.6 mg of **1** was dissolved in 0.5 mL of water, and 5 µL of this solution was applied dropwise to the GCE. Finally the target-modified electrode **1/GCE** was obtained by drying overnight at room temperature. **SbW<sub>9</sub>/GCE** was prepared by the same method, however, Na<sub>9</sub>[SbW<sub>9</sub>O<sub>33</sub>]·19.5H<sub>2</sub>O was used instead of compound **1**.

### Experimental materials

Na<sub>9</sub>[SbW<sub>9</sub>O<sub>33</sub>]·19.5H<sub>2</sub>O was synthesized according to the literature method.<sup>1</sup> Other raw materials were analytical grade reagents, all of which were obtained from commercial sources and used without further purification.

### X-Ray crystallographic analysis

The single-crystal X-ray diffraction data for **1** were collected on a Bruker APEX Duo2 CCD diffractometer, using a Mo K $\alpha$  radiation with  $\lambda = 0.71073 \text{ \AA}$ , under nitrogen atmosphere and at 175 K. The empirical absorption correction was based on equivalent reflections. The crystal structures were solved by the direct method and refined by the full-matrix least-squares method on  $F^2$  according to the SHELX and OLEX 2. The residual electron density that could not be reasonably modelled as solvents or cations was removed by applying the SQUEEZE function in PLATON.<sup>3</sup> The final formula of **1** were determined by the combining single-crystal X-ray diffractions with the elemental analysis, thermogravimetric analysis and charge balance. Crystallographic data for the structures reported have been deposited in the Cambridge Crystallographic Data Centre with CCDC reference number 2290806 for compound **1**, respectively. These data can be obtained free of charge from the Cambridge Crystallographic Data Centre at [www.ccdc.cam.ac.uk/data\\_request/cif](http://www.ccdc.cam.ac.uk/data_request/cif). The selected crystal parameters, data collection, and refinements are summarized in **Table S1**.

### Synthetic Discussion

The organic 1,1'-bis(3-carboxylatobenzyl)4,4'-bipyridinium) dichloridelig and did not occur in the final structure. We attempted to remove the ligand for crystal growth, but unfortunately did

not obtain the corresponding compounds. Due to the presence of carboxyl groups in the ligand, it may play a role in regulating the pH or influencing the solution environment during the reaction process.

## 2. Additional Tables

**Table S1** Crystal data and structure refinement parameters for **1**

Compound	<b>1</b>
Empirical formula	KNa <sub>1.5</sub> Nd <sub>6</sub> O <sub>144</sub> Sb <sub>4</sub> W <sub>36</sub>
$M_r$ (g·mol <sup>-1</sup> )	10388.12
Temperature (K)	175
Crystal system	monoclinic
Space group	$P2_1$
$a$ (Å)	29.023(6)
$b$ (Å)	21.827(4)
$c$ (Å)	33.519(7)
$\alpha$ (°)	90.00
$\beta$ (°)	90.856(8)
$\gamma$ (°)	90.00
$V$ / Å <sup>3</sup>	21232(7)
$Z$	4
$\rho_{\text{calcd}}$ (g/cm <sup>3</sup> )	3.237
$\mu$ (mm <sup>-1</sup> )	21.443
$F(000)$	17662.0
$2\theta$ range / °	1.87 to 50.456
$R_{\text{int}}$	0.1111
GooF	1.012
$R_1^{[a]}$ [I > 2 $\sigma$ ]	$R_1^a = 0.0502$
	$wR_2^b = 0.1177$
$R_1$ (all data)	$R_1^a = 0.0624$
	$wR_2^b = 0.1231$

$$^{[a]}R_1 = \sum ||F_o| - |F_c|| / \sum |F_o|, \quad ^{[b]}wR_2 = \{ \sum [w(F_o^2 - F_c^2)^2] / \sum [w(F_o^2)^2] \}^{1/2}.$$

**Table S2** Analytical performance of amperometric sensors based on polyoxotungstates for detection of bromate.

Compounds	Sensitivity (μA·mM <sup>-1</sup> )	Linear range (mM)	LOD (μM)	Ref
C <sub>80</sub> H <sub>116</sub> Ag <sub>4</sub> N <sub>10</sub> O <sub>68</sub> SiW <sub>12</sub>	12.66	0.12–5.8	5.6	4
C <sub>64</sub> H <sub>48</sub> Ag <sub>3</sub> N <sub>8</sub> O <sub>40</sub> PW <sub>12</sub>	101.7	3.4–8.0	16.9	
MENU-3	45.11	0.005–0.56	0.55	5
MENU-5	18.63	0.015–0.38	1.18	
[Ni <sub>4</sub> (P <sub>8</sub> W <sub>48</sub> O <sub>184</sub> )(WO <sub>2</sub> ) <sub>28</sub> ] <sup>-</sup>	69.4	0.1–2.0	20	6
CoW <sub>11</sub> Co/PVP/TiO <sub>2</sub>	-	0.02–4.4	5.0	7

$[\text{SiNi}(\text{H}_2\text{O})\text{W}_{11}\text{O}_{39}]^{6-}$	-	0.014–13.85	14.88	8
$\text{C}_{44}\text{H}_{72}\text{Ag}_4\text{N}_{16}\text{O}_{44}\text{SiW}_{12}$	6.01	0.012–0.08	31	9
NENU-3	51.9	0.05–19.1	12	10
$[(\text{Cu}_2(\text{H}_2\text{bdpm})_2)[\text{H}_2\text{P}_2\text{W}_{18}\text{O}_{62}]_{0.5}] \cdot 2\text{H}_2\text{O}$	201.53	0.02–0.048	18	11
<b>Compound 1</b>	<b>186</b>	<b>0.0047–2.4</b>	<b>1.9</b>	<b>this work</b>

**Table S3** Determination results and the recoveries of bromate in tap water (n = 5).

Sample	Found ( $\mu\text{M}$ )	Added ( $\mu\text{M}$ )	Total found ( $\mu\text{M}$ )	Average ( $\mu\text{M}$ )	RSD (%)	Recovery (%)
Tap water	-	30.0	30.8, 27.7, 29.9, 27.9, 29.8	29.2	4.8	97.3
		100	108, 107, 101, 102, 107	105	3.0	105
		500	523, 530, 536, 525, 523	527	1.1	106

### 3. Additional Figures

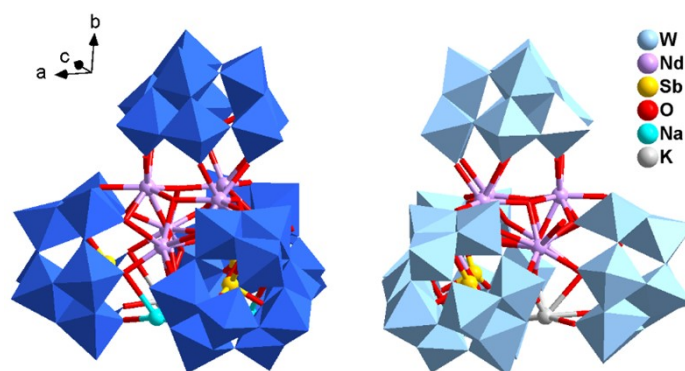


**Fig. S1** View of the two crystallographically independent  $\{\text{Nd}_6(\text{OH})_6(\text{H}_2\text{O})_6(\text{B-}\alpha\text{-SbW}_9\text{O}_{33})_4\}$  (**1a**) polyanion clusters in compound **1**.

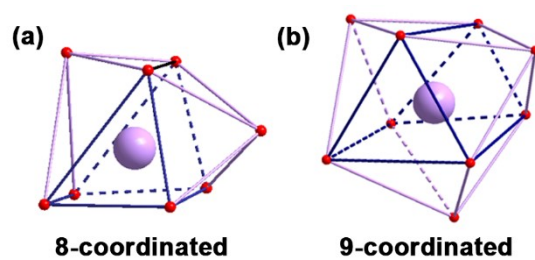


**Fig. S2(a)** The dicapped trigonal prism of the 8-coordinated  $\text{Nd}^{3+}$ ; **(b)** The distorted tricapped trigonal prism of the 9-coordinated  $\text{Nd}^{3+}$ .

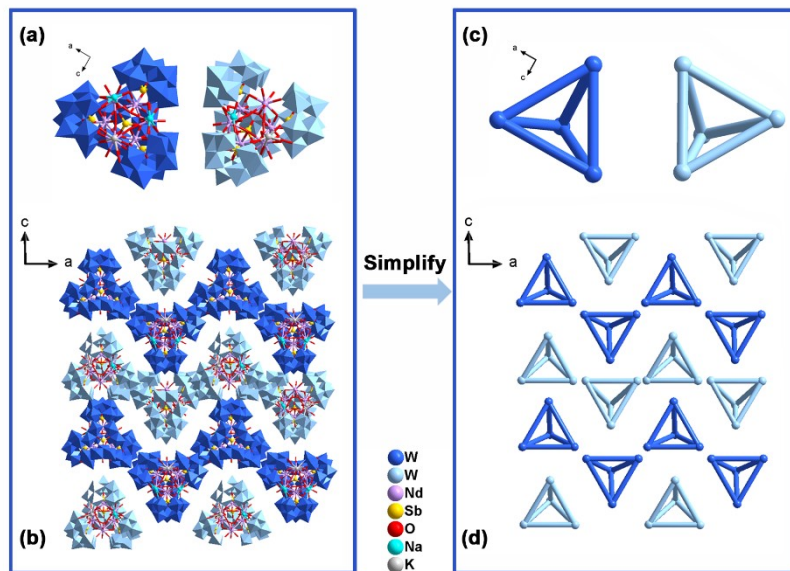


**Fig. S3** (a) View of two kinds of **1a** with different alkali metal ions:  $\{KNa_2(\mathbf{1a})\}$  (left) and  $\{KNa(\mathbf{1a})\}$  (right); (b) View of the packing arrangement of **1** along the *b* axis; (c) Simplified diagram of two kinds of **1a**; (d) Simplified diagram of packing arrangement of **1**.

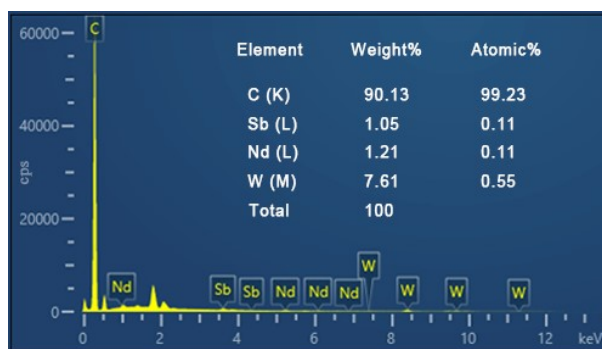


**Fig. S4** EDS analysis of **1/GCE** showing the presence of C, Sb, Nd, and W elements.

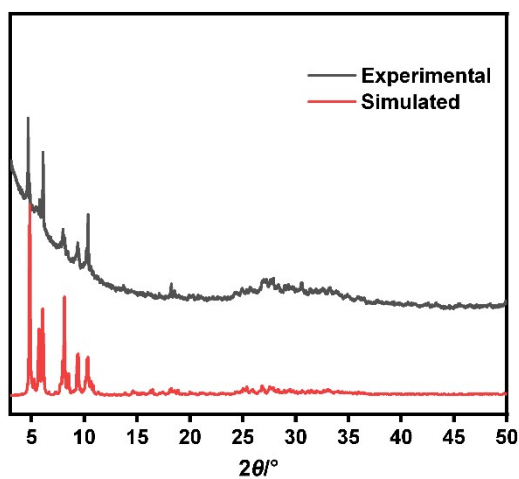


**Fig. S5** Simulated and experimental PXRD patterns of **1**

The phase purity of **1** was confirmed by powder X-ray diffraction (PXRD) measurement (Fig. S5). The result shows that the experimental peaks matched well with the simulated values,

indicating that there are no impurities in the sample.

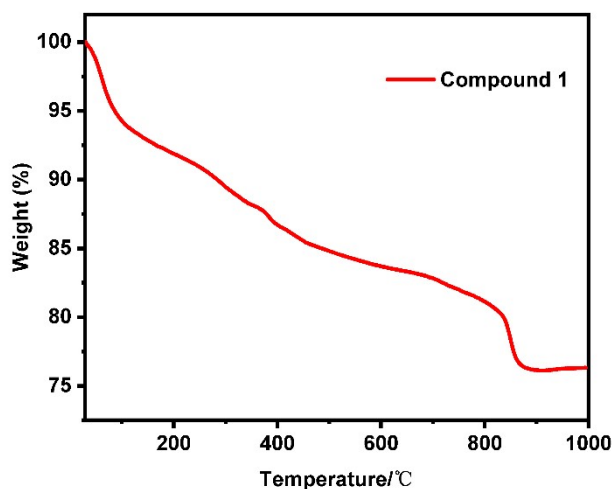


Fig. S6 TG curve of 1.

To investigate the stability of 1 during heating, Thermal gravimetric analysis (TGA) of 1 was performed under nitrogen atmosphere in the range of 30–1000 °C at a heating rate of 10 °C/min. As shown in Figure S6, the TG curve shows a three-step weight loss. Thermogravimetric analysis shows that the first continuous weight loss from room temperature to 100 °C is about 5.8%, which may be related to the loss of 67 lattice water molecules. Subsequently, there was a weight loss of approximately 0.3% at 370–390 °C, which is due to the loss of 12 coordinated water molecules. The crystal undergoes a continuous weight loss between 400 and 800 °C, and finally, the skeleton decomposed at approximately 830 °C.

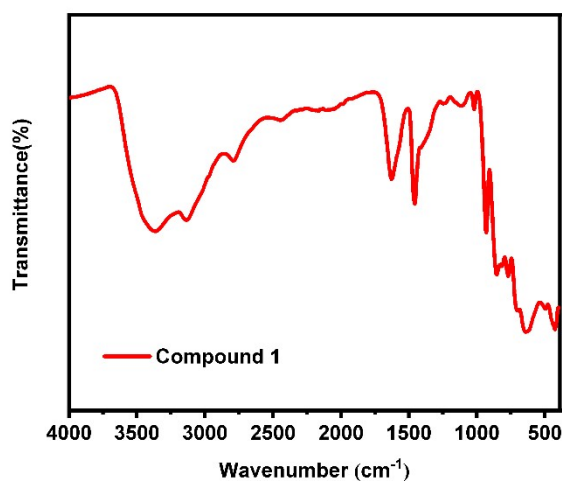


Fig.S7 IR spectrum of the 1

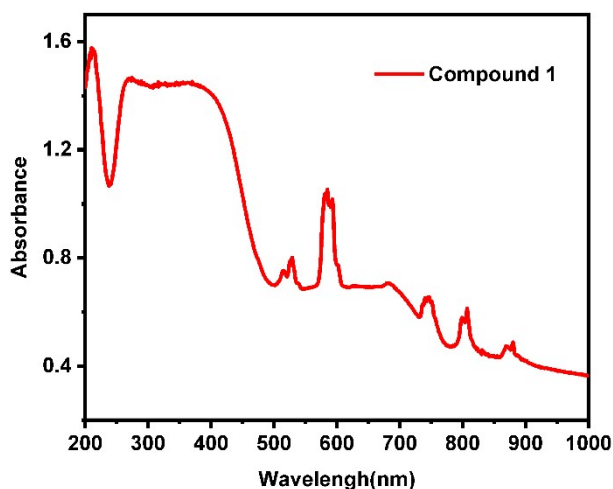


Fig. S8 The solid UV-vis absorption spectra for **1**

UV absorption spectroscopy of compound **1** was examined in the 200-1000 nm region. As shown in Fig. S8, there is a broad absorption peak in the range of about 200-400 nm, which can be attributed to the charge transfer transition of O-W in **1**. Due to the presence of  $\text{Nd}^{3+}$ , a characteristic absorption peak of  $\text{Nd}^{3+}$  is observed in the spectrum. Peaks at 515, 529 and 585 nm correspond to the  ${}^4\text{I}_{9/2}\text{-}{}^4\text{G}_{9/2}$ ,  ${}^4\text{I}_{9/2}\text{-}{}^4\text{G}_{7/2}$  and  ${}^4\text{I}_{9/2}\text{-}{}^4\text{G}_{5/2}$  transitions, respectively. Small peaks at 629 nm are due to the  ${}^4\text{I}_{9/2}\text{-}{}^4\text{H}_{11/2}$  transition. Peaks at 684, 743, 752, 805 and 875 nm correspond to the  ${}^4\text{I}_{9/2}\text{-}{}^4\text{F}_{9/2}$ ,  ${}^4\text{I}_{9/2}\text{-}{}^4\text{F}_{7/2}$ ,  ${}^4\text{I}_{9/2}\text{-}{}^4\text{S}_{3/2}$ ,  ${}^4\text{I}_{9/2}\text{-}{}^4\text{F}_{5/2}$  and  ${}^4\text{I}_{9/2}\text{-}{}^4\text{F}_{3/2}$  transitions, respectively.

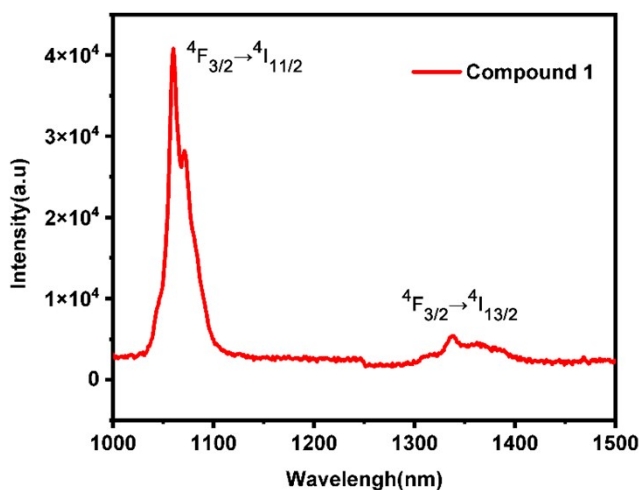
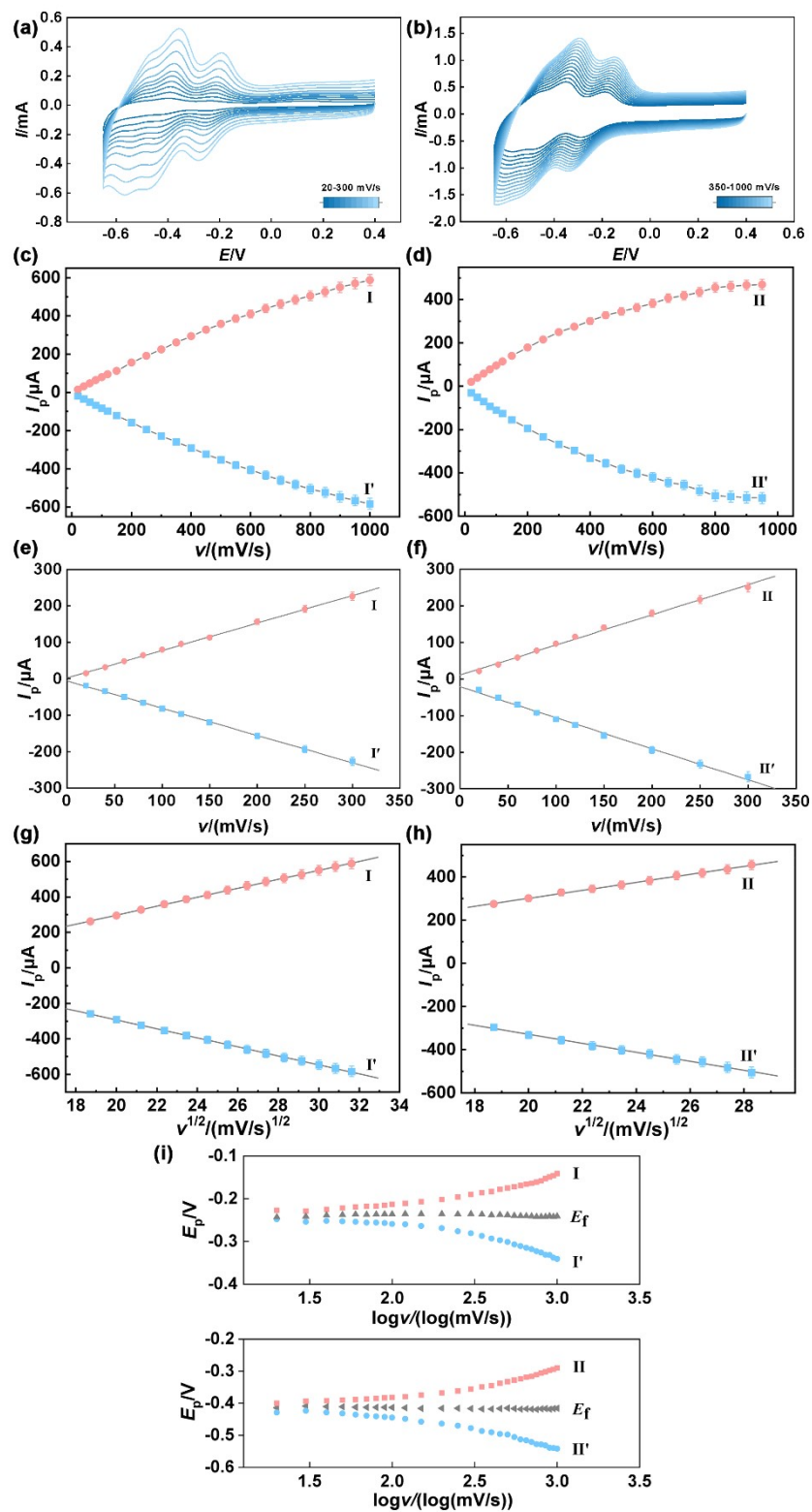
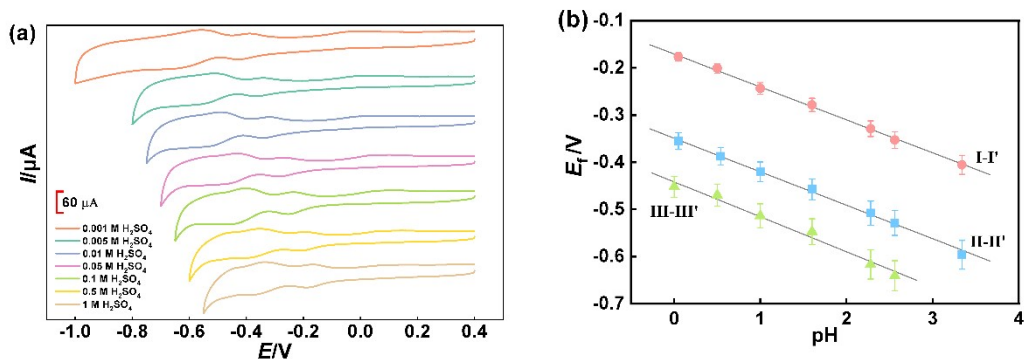


Fig. S9 The emission spectrum of **1**.

Under 808 nm excitation, compound **1** displays characteristic emission bands of  $\text{Nd}(\text{III})$  in the near-infrared region. In Fig. S9, the strong band at 1064 nm, and the weak band at 1334–1380 nm at 1064 nm are attributed to the  ${}^4\text{F}_{3/2}\text{-}{}^4\text{I}_{11/2}$  and  ${}^4\text{F}_{3/2}\text{-}{}^4\text{I}_{13/2}$  transition of  $\text{Nd}(\text{III})$  ions, respectively.



**Fig. S10** CV curves of 1/GCE in 0.1 mol/L H<sub>2</sub>SO<sub>4</sub> in potential scan rate range of 20-300 mV/s (a), and in 350-1000 mV/s (b); (c, d) plots of peak currents versus scan rate in 20-1000 mV/s of I-I' and II-II'; (d, e) the linear plots between peak currents and scan rate in 20-300 mV/s of I-I' and II-II'; (f, g) the linear plots between peak currents and the square root of scan rate in 350-1000 mV/s of I-I' and II-II'; (h, i) plots between peak potential and log v in 20-1000 mV/s.



**Fig. S11** (a) Variation of the cyclic voltammogram of 1/GCE in  $\text{H}_2\text{SO}_4 + \text{Na}_2\text{SO}_4$  with different pH; (b) variation of the formal potentials  $E_f$  as a function of pH of the I-I', II-II' and III-III' redox waves. The supporting electrolyte, 0.001, 0.005, 0.01, 0.05, 0.1, 0.5 and 1.0 mol/L  $\text{H}_2\text{SO}_4 + 0.1$  mol/L  $\text{Na}_2\text{SO}_4$ , potential scan rate 20 mV/s.

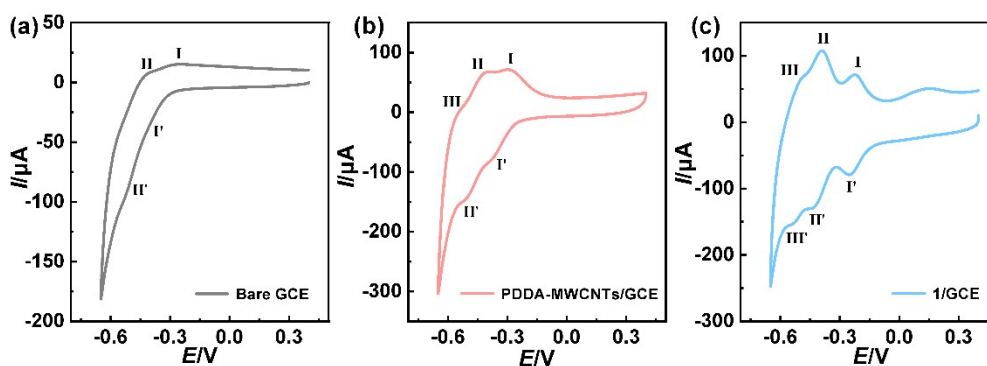


**Fig.S12** (a, b) CV curves of 0.1 mmol/L POM 1 solution on bare GCE and PDDA-MWCNTs/GCE in 0.1 mol/L  $\text{H}_2\text{SO}_4$ , respectively; (c) CV curve of 1/GCE in 0.1 mol/L  $\text{H}_2\text{SO}_4$ , the potential scan rate 50 mV/s.

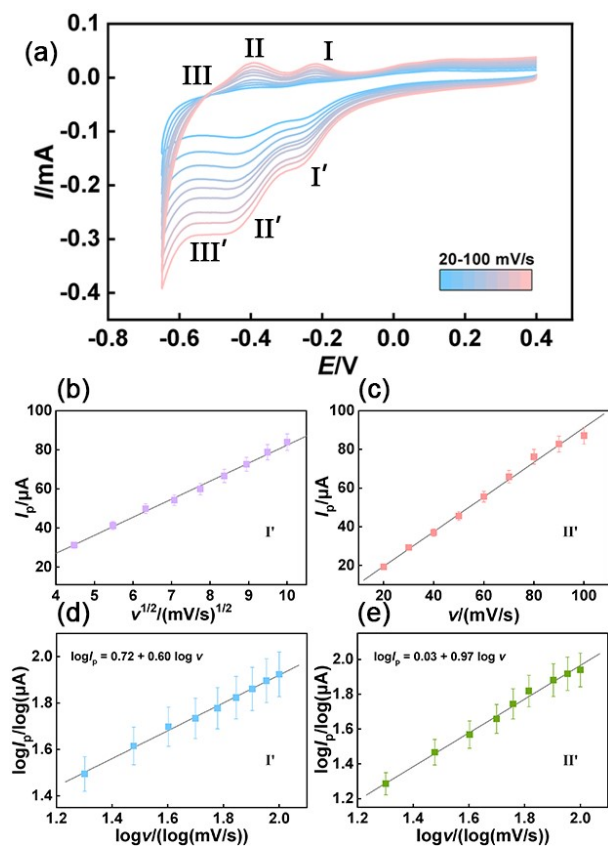


**Fig. S13** (a) CV curves of 1/GCE at various potential scan rate with the addition of 2.0 mM bromate, (b)  $I_p$ - $v^{1/2}$  plot of reduction peak I' from (a), (c)  $I_p$ - $v$  plot of reduction peak II' from (a), (d)  $\log I_p$ - $\log v$  plot of reduction peak I' from (a), (e)  $\log I_p$ - $\log v$  plot of reduction peak II' from (a), the supporting electrolyte, 0.1 mol/L H<sub>2</sub>SO<sub>4</sub>.

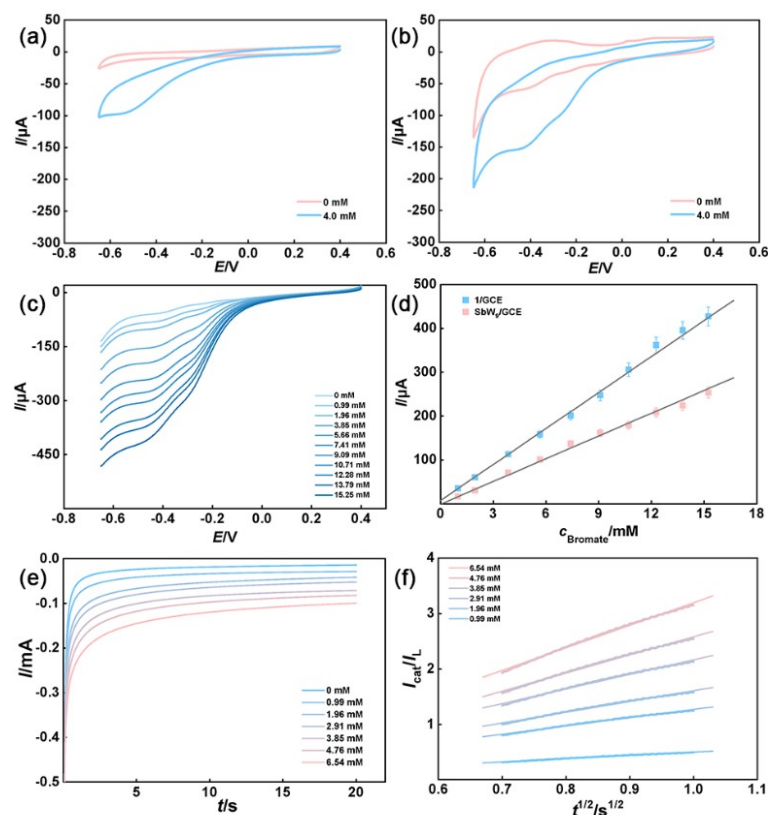


**Fig. S14** (a) CV curves of PDDA-MWCNTs/GCE with 4.0 mM bromate added; (b) CV curves of SbW<sub>9</sub>/GCE with 2.0 mM bromate added; (c) CV curves (cathode branch only) of SbW<sub>9</sub>/GCE with various concentration of bromate; (d) The calibration plots between the catalytic current (measured at -0.30 V) to bromate concentration; (e) CA curves of SbW<sub>9</sub>/GCE with the addition different concentration of bromate; (f) The linear relationships of  $I_{cat}/I_L$  value versus  $t^{1/2}$  of SbW<sub>9</sub>/GCE; potential scan rates of CV: 20 mV/s.

## Notes and references

- [1] M. Bösing, I. Loose, H. Pohlmann and B. Krebs, *Chem.--Eur. J.*, 1997, **3**, 1232-1237.
- [2] (a) G. M. Sheldrick. *Acta Cryst.*, 2008, **A64**, 112–122. (b) G. M. Sheldrick, *Acta Cryst.*, 2015, **C71**, 3–8.
- [3] (a) A. L. Spek, *Acta. Cryst.*, 2015, **71**, 9-18.; (b) P. Sluis, and A. L. Spek, *Acta Crystallogr. Sect. A*. 1990, **46**, 194-201.
- [4] A. X. Tian, J. N. Liu, T. T. Li, Y. Tian, G. Y. Liu and J. Ying, *CrystEngComm*, 2018, **20**, 2940-2951.
- [5] Y. N. Zhang, Y. Zhang, L. Li, J. L. Chen, P. Z. Li and W. H. Huang, *J. Electroanal. Chem.*, 2020, **861**, 113939.
- [6] B. Ali, F. Laffir, L. Kailas, G. Armstrong, L. Kailas, R. O'Connell and T. McCormac, *Eur. J. Inorg. Chem.*, 2019, **2019**, 394-401.
- [7] Y. C. Li, W. F. Bu, L. X. Wu and C. Q. Sun, *Sens. Actuators. B*, 2005, **107**, 921-928.
- [8] C. Y. Chen, Y. H. Song and L. Wang, *Electrochimica Acta.*, 2009, **54**, 1607-1611.
- [9] A. X. Tian, M. L. Yang, N. Sun, Y. B. Fu and J. Ying, *Polyhedron*, 2018, **155**, 337-350.
- [10] E. B. Shi, X. Q. Zou, J. Liu, H. M. Lin, F. Zhang, S. X. Shi, F. H. Liu, G. S. Zhu and F. Y. Qu, *Dalton Trans.*, 2016, **45**, 7728-7736.
- [11] A. X. Tian, M. L. Yang, H. P. Ni, N. Sun, Y. Yang, Y. B. Fu and J. Ying, *Transit. Met. Chem.*, 2018, **43**, 621-633.